ACS SENSORS

Article

Cite This: *ACS Sens.* 2019, 4, 1577−1585

pubs.acs.org/acssensors

Mechanism of Sensitivity Enhancement of a ZnO Nanofilm Gas Sensor by UV Light Illumination

Gaoda Li,[†,#] Zhe Sun,[†,#] Dongyi Zhang,[†] Qi Xu,[‡] Leixin Meng,[†] and Yong Qin*[,†,‡]

[†]Institute of Nanoscience and Nanotechnology, School of Physical Science and Technology, Lanzhou University, Lanzhou, 730000, China

[‡]School of Advanced Materials and Nanotechnology, Xidian University, Xi'an, 710071, China

ABSTRACT: Although ultraviolet (UV) light illumination has been widely used to increase the sensitivity of semiconductor gas sensors, its underlying mechanism is still blurred and controversial. In this work, the influence of UV light illumination on the sensitivity of ZnO nanofilm gas sensors is explored experimentally and simulated based on a modified Wolkenstein's model. The influential factors on sensitivity are determined respectively: the surface band bending and Fermi level are measured by Kelvin probe force microscopy, the binding energy and extrinsic surface state are calculated by density functional theory, and the depletion of the whole semiconductor caused by the finite size is illustrated by the transfer characteristics of a field effect transistor. With all these factors taken into consideration, the surface state densities of adsorbed O_2 and NO_2 molecules in the dark and under UV light illumination are calculated which determine the sensitivity. Good agreement has been obtained between the experiment and simulation results. Accordingly, when NO_2 is introduced into the atmosphere, the enhancement of sensitivity is ascribed to the more dramatic increase of surface state density and surface band bending activated by the UV light illumination compared with that in the dark. This finding is critical and would contribute greatly to the development of gas sensors with high sensitivity.

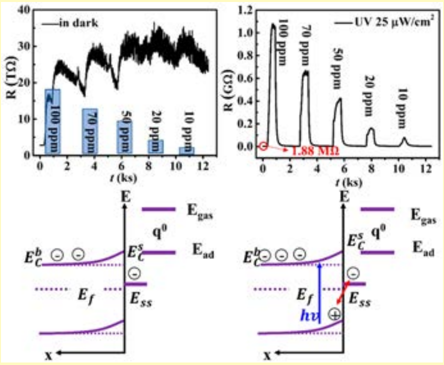

KEYWORDS: *gas sensor, adsorption, UV enhancement, sensing mechanism, ZnO*

In recent years, increasing attention about gas sensors has been paid to semiconductor oxide nanomaterials, represented by ZnO nanowires,[1−4] polycrystalline[5−8] and nanofilm.[7−14] To enhance the sensitivity and lower the operating temperature of gas sensors, illumination with UV light has been proven to be a promising method.[5,15−17] When illuminated with UV light with energy larger than the band gap of ZnO (3.37 eV), photocarriers are generated which could influence the adsorption and desorption processes of gas molecules. Although widely used, the enhancement of a gas sensor's sensitivity by UV light illumination is explained by contradictory mechanisms. (1) The combination of photogenerated holes and the negatively charged adsorbed oxygen ions leads to the decrease of the surface depletion layer, while the remaining photogenerated electrons reacted with NO_2 molecules, which widens the surface depletion region. As a result, the UV light illumination results in the desorption of O_2 and the adsorption of NO_2.[12] (2) Because of the reaction of photogenerated electrons and ambient oxygen molecules, more active oxygen ions are created and react with the reducing gas molecules, which leads to the increase of sensitivity.[5,13,17,18] (3) More oxygen ions are produced due to the photogenerated electrons, which react with the NO_2 molecules.[19,20] (4) NO_2 would extract electrons from photoinduced oxygen ions due to the stronger electron affinity of NO_2 molecules compared with that of O_2.[9]

This contradiction in different mechanisms is caused by the arbitrarily assumed increase or decrease of adsorbed molecules when the gas sensor is illuminated by UV light. To clarify the underlying mechanism of the UV light enhancement of the gas sensor's sensitivity, the influence of UV light illumination on the surface state densities of adsorbed O_2 and NO_2 molecules should be quantified, which could modify the corresponding surface barrier height and carrier concentration. According to Wolkenstein's model of chemisorption on semiconductors, the surface state density of adsorbed molecules is influenced by the binding energy, extrinsic surface state caused by adsorption, Fermi level, surface barrier height, and partial pressure of gas.[21] Furthermore, the surface band bending and Fermi level are also modulated by the size of semiconductor; when the size of nanoparticle is smaller than the depletion width, the whole nanoparticle would be depleted, and the carrier concentration would dramatically decrease, as we have previously clarified.[22] When illuminated by UV light, photogenerated carriers are induced, and a new equilibrium of surface state density is obtained.[23] Only when all these factors are taken into consideration, the enhancement of gas sensor's sensitivity by UV light illumination could be clarified.

Received: February 3, 2019
Accepted: May 8, 2019
Published: June 5, 2019

ACS Publications

DOI: 10.1021/acssensors.9b00259
ACS Sens. 2019, 4, 1577−1585

In this paper, the enhancement of sensitivity of a ZnO nanofilm NO_2 gas sensor by UV light illumination is simulated based on a modified Wolkenstein's model and space charge model. The factors mentioned above are determined experimentally or numerically: the surface band bending and Fermi level are measured by Kelvin probe force microscopy (KPFM), the binding energy and extrinsic surface state are calculated by density functional theory (DFT), and the depletion of whole semiconductor caused by the finite size is illustrated by the transfer characteristics of a field effect transistor (FET). With all these factors taken into consideration, the surface state densities of adsorbed O_2 and NO_2 molecules in the dark and under UV light illumination are calculated respectively, which determine the sensitivity. The enhancement of the sensitivity of a ZnO nanofilm gas sensor by UV light illumination is simulated and compared with the experimental results. According to the simulation and experimental results, when NO_2 is introduced into the atmosphere, the enhancement of sensitivity is ascribed to the more dramatic increase of surface state density and surface band bending led by the UV light illumination compared with that in the dark.

■ RESULTS AND DISCUSSION

Modified Wolkenstein's Model. According to Wolkenstein's model of chemisorption on semiconductors, the adsorption of gas molecules on a semiconductor surface is divided into "weak" and "strong" forms, as indicated by Figure 1.[21,23] At the beginning of adsorption, the surface of semiconductor is neutral, and its energy band is flat. The energy of adsorbed molecules decreases by the binding energy, $q^0 = E_{gas} - E_{ad}$, corresponding to the weak adsorption form. Extrinsic surface states located at E_{ss} are also created by the adsorption and serve as traps for electrons, as shown in Figure 1a. The transfer of electron from the conduction band E_C to the extrinsic surface state E_{ss} leads to the depletion of electrons near the surface and negatively charged adsorbates at the surface. Meanwhile, the energy of the system decreases by $E_C^b - E_{ss}$ (E_C^b denotes the conduction band at the bulk), which corresponds to the strong adsorption form, as indicated by Figure 1b. Because of the finite size of the semiconductor, the further transfer of electrons leads to the depletion of the whole semiconductor, which results in the enlargement of the distance between the Fermi level and conduction band. At equilibrium, the Fermi level is below the extrinsic surface state, which limits the transfer of electrons and results to the equilibrium of adsorption, as shown in Figure 1c. The UV light illumination leads to the photogenerated carriers, and the extra holes transfer to the surface due to the inner electric field. The combination of extra holes and the adsorbed ions results to a new equilibrium under UV light illumination, as illustrated by Figure 1d. The equilibrium is governed by the following equations:

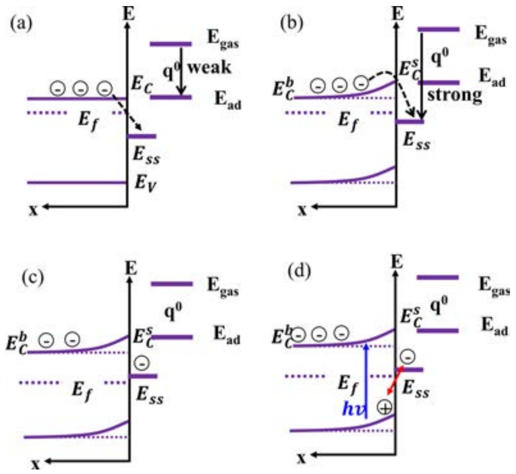

Figure 1. Chemisorption of acceptor-type molecules on a n-type semiconductor: (a) "weak" adsorption at the beginning of adsorption with a flat energy band; (b) "strong" adsorption leads to the charge transfer and surface band bending; (c) at equilibrium, the depletion of the whole semiconductor caused by the finite size of the semiconductor results in the enlargement of the distance between the Fermi level and conduction band, and the Fermi level is below the extrinsic surface state; (d) the combination of photogenerated holes and the adsorbed ions results in a new equilibrium under UV light illumination. $q^0 = E_{gas} - E_{ad}$ is the binding energy of the gas molecules, E_f, E_C^b, E_C^s, E_V, and E_{ss} are the Fermi level, conduction band at the bulk, conduction band at the surface, and the valence band, respectively.

$$\alpha p(N^* - N^- - N^0) = \nu^0 N^0 \exp\left(-\frac{q^0}{k_B T}\right) + \nu^- N^- \exp\left(-\frac{q^0 + E_C^b - E_{ss}}{k_B T}\right) \tag{1}$$

$$\frac{N^-}{N^- + N^0} = \frac{1}{1 + \exp\left(-\frac{E_f - E_{ss}}{k_B T}\right)} \tag{2}$$

$$\alpha = \frac{k}{N^* \sqrt{2\pi M k_B T}} \tag{3}$$

where N^* is the number of adsorption sites per unit surface area, N^0 is the number of neutral/weak adsorbates per unit area, N^- is the number of negative/strong adsorbates per unit area, i.e., the surface state density, q^0 is the binding energy of adsorption, p is the ambient gas pressure, M is the mass of a gas molecule, k_B is the Boltzmann constant, T is the temperature, ν^0 and ν^- are the oscillation frequencies of the corresponding adsorbates (ν^0 and $\nu^- = 10^{13}$ Hz), and k is the condensation coefficient, which equals 0.2.[21]

Taking the variation of electron and hole's concentration into consideration, the kinetics of surface state density follows the following equations:

$$\frac{dN^0}{dt} = (a_1 - a_2) - [(b_1 + b_4) - (b_2 + a_3)] \tag{4}$$

$$\frac{dN^-}{dt} = (b_1 + b_4) - (b_2 + a_3) \tag{5}$$

$$a_1 = \frac{k}{N^* \sqrt{2\pi M k_B T}} p(N^* - N^- - N^0) \tag{6}$$

$$a_2 = \nu^0 N^0 \exp\left(-\frac{q^0}{k_B T}\right) \tag{7}$$

$$b_1 = \beta_1 n_s N^0 \tag{8}$$

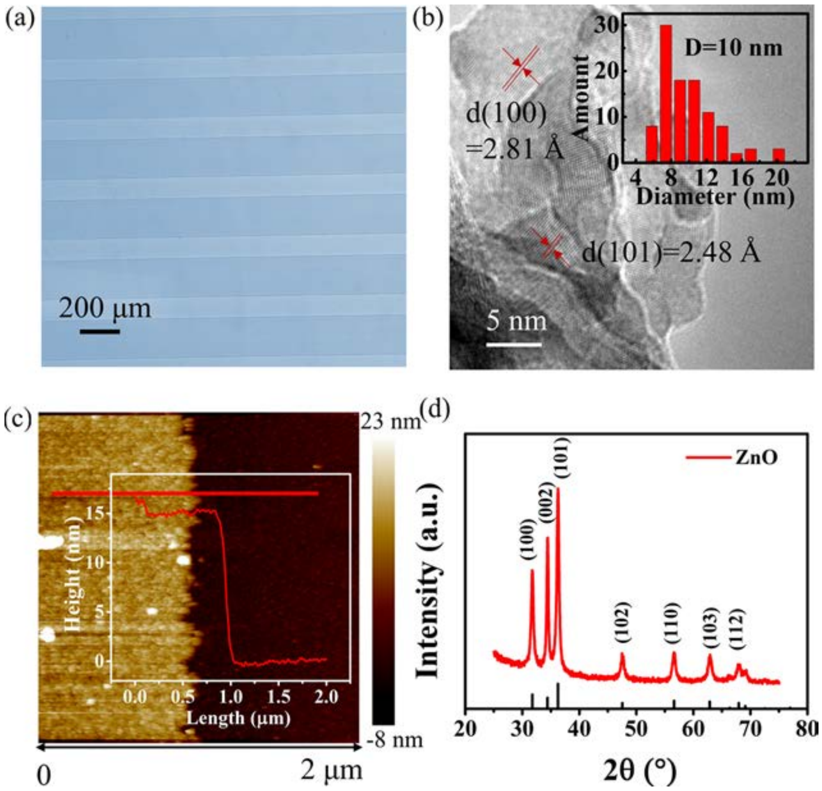

Figure 2. ZnO nanofilm gas sensor and the characterization of ZnO nanofilm: (a) the optical picture of the ZnO gas sensor; (b) HRTEM reveals the ZnO nanoparticle's high degree of crystallinity, and the inset shows the size distribution of ZnO nanoparticles is between 6 and 20 nm, with an average diameter of 10 nm; (c) AFM characterization indicates that the average thickness of ZnO nanofilm is 15 nm, and the red line is the position of the measurement shown in the inset; (d) the X-ray diffraction pattern shows that ZnO film is polycrystalline and exhibits no preferred orientation.

$$b_2 = \beta_2 N^- \exp\left(-\frac{E_C^s - E_{ss}}{k_B T}\right) \tag{9}$$

$$b_3 = \beta_3 p_s N^- \tag{10}$$

$$b_4 = \beta_4 N^0 \exp\left(-\frac{E_{ss} - E_V^s}{k_B T}\right) \tag{11}$$

where a_1 and a_2 denote the number of gas molecules that adsorb and desorb per unit time on and from a unit surface area of the semiconductor. b_1, b_2, b_3, and b_4 denote the number of electron transitions per unit time per unit surface area: b_1 refers to the transition of electron from the conduction band to the extrinsic surface state (b_2 is the reverse); b_3 refers to the transition from surface state to the valence band (b_4 is the reverse). n_s (p_s) denotes the electron (hole) density at surface, E_C^s (E_V^s) is the conduction (valence) band at surface. β_1 ,β_2, β_3, and β_4 are the corresponding coefficients of the transitions.

In equilibrium, eqs 1 and 2 should equal to zero. Since ZnO is a n-type semiconductor, b_4 could be omitted due to the large $E_{ss} - E_V^s$, and the hole density at surface could be replaced as the photogenerated hole density. The resulting equilibrium is

$$\beta_1 n_s \alpha p N^* = \left[\beta_1 n_s \alpha p + \beta_2 \exp\left(-\frac{E_C^s - E_{ss}}{k_B T}\right) X + \beta_3 p_s X\right] N^- \tag{12}$$

$$X = \alpha p + v^0 \exp\left(-\frac{q^0}{k_B T}\right) \tag{13}$$

$$n_s = N_C \exp\left(-\frac{E_C^s - E_f}{k_B T}\right) \tag{14}$$

$$p_s = \alpha \frac{I}{hv}(1 - R)\tau \tag{15}$$

where X is an intermediate variable, N_C ($3.0 \times 10^{18}/\text{cm}^3$) is the effective density of states in the conduction band of ZnO,[17] α is the adsorption coefficient equals 7.1×10^4/cm when the wavelength of UV light is 365 nm,[24] I is the UV light intensity, 25 μW/cm^2 in our experiment, hv is the photon energy of UV light and 365 nm wavelength corresponds to 3.40 eV, R is the reflective coefficient, omitted in our calculation, and τ is the carrier lifetime (14 ns).[25]

Comparing the above equations with the original equilibrium described by eqs 1−3, the following relation is obtained:

$$\frac{\beta_1}{\beta_2} = 1 + \frac{v^-}{\alpha p} \exp\left(-\frac{q^0 + E_C^b - E_{ss}}{k_B T}\right) \tag{16}$$

From the above model, it is demonstrated that the surface state density of adsorbed molecules is determined by the following factors: partial pressure of gas p, binding energy q^0, surface band bending $E_C^s - E_C^b$, position of surface state $E_C^s - E_{ss}$, the position of Fermi level $E_C^s - E_f$, and the photogenerated hole

DOI: 10.1021/acssensors.9b00259
ACS Sens. 2019, 4, 1577−1585

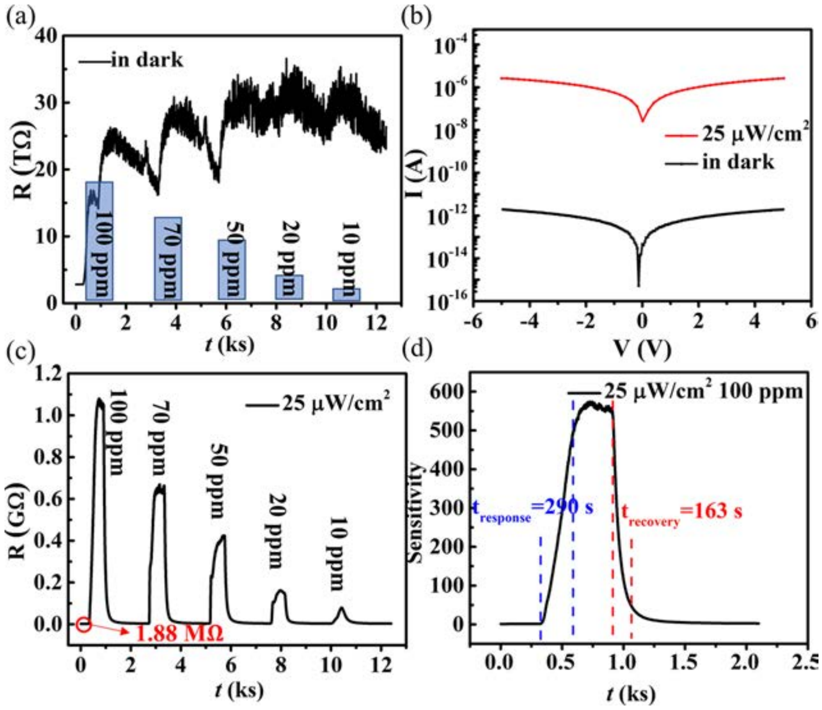

Figure 3. Response of ZnO nanofilm gas sensor in different situations: (a) in the dark, the sensor has a low sensitivity and a slow response to different concentration of NO_2 (mixed with air); (b) due to the depletion of whole nanofilm, ZnO nanofilm exhibits a sensitivity with 6 orders of magnitude to UV light illumination; (c) the illumination of UV light leads to a dramatic increase in the sensitivity to different concentrations of NO_2; (d) the response and recovery time are also reduced by the UV light illumination.

density p_s. These factors are further determined by the following sections.

Materials and Methods. ZnO nanofilm is synthesized by the spin-coating method.[26] ITO interdigital electrodes are sputtered on the top of quartz glass substrate by photolithography and magnetron sputtering. Precursor solution is further spin-coated on the top of the substrate. By heating at 150 °C for 2 h, the dense, high-quality, polycrystalline ZnO film gas sensor is fabricated. The distance between electrodes is 300 μm, as shown in Figure 2a. High-resolution TEM (HRTEM) characterization indicates an interplanar spacing of 0.281 nm of the ZnO nanoparticle, which corresponds to the distances between ZnO(100) facets, and a spacing of 0.248 nm refers to the distances between ZnO(101) facets, as shown in Figure 2b. The inset shows the size distribution of ZnO nanoparticles is between 6 and 20 nm, with an average diameter of 10 nm. Further characterization of ZnO nanofilm by AFM indicates the film is composed of nanoparticles and the thickness of nanofilm measures 15 nm by a cross section across the ZnO nanofilm and the substrate, indicated as the red line in Figure 2c and shown in the inset. Because of the thickness of the ZnO nanofilm (15 nm), its direct X-ray diffraction pattern is unavailable. By sequential coatings, a thicker ZnO film is obtained, and its X-ray diffraction pattern is shown in Figure 2d, which is consistent with the pattern of hexagonal wurtzite structure. From the X-ray diffraction pattern, it is observed that ZnO film is polycrystalline and has no preferred orientation.

The response of ZnO nanofilm to NO_2 gas (mixed with air) is measured, and the sensitivity (S_1) is determined by dividing the resistance of ZnO nanofilm (R_{gas}) in NO_2/air mixed gas by the resistance of ZnO nanofilm (R_{air}) in the presence of air. As shown in Figure 3a, the ZnO nanofilm without UV light illumination has a really small sensitivity, only 10 when the concentration of NO_2 is 100 ppm, and the recovery of the resistance when the gas is replaced by air is really slow. When illuminated by UV light with 365 nm wavelength and 25 μW/cm^2 intensity, the resistance of ZnO nanofilm dramatically decreases, and the sensitivity (S_2) is 1.4×10^6, which is determined by dividing the current of ZnO nanofilm under UV light by that in the dark, as shown in Figure 3b. This dramatic decrease of resistance led by UV light illumination is induced by the depletion of whole nanofilm by the adsorbed O_2 molecules, as further illustrated afterward. Under UV light illumination, the sensitivity (S_3) of ZnO nanofilm to NO_2 gas dramatically increases, as shown in Figure 3c. The sensitivity increases from 10 in the dark to 575 under 25 μW/cm^2 UV light with the same NO_2 concentration of 100 ppm. The illumination of UV light also leads to a much faster response and recovery time, 290 and 163 s respectively, as shown in Figure 3d.

Because of the finite particle size of the ZnO nanofilm, the adsorption of oxygen molecules at surface leads to the depletion of whole nanofilm, which results in the enlargement of the distance between the Fermi level and conduction band, as illustrated in Figure 1. To indicate this effect, FET made of ZnO nanofilm is characterized. The distance between interdigital electrodes is 300 μm, as shown in Figure 4a. The transfer characteristics of the same FET with and without oxygen adsorbed are compared. As shown in Figure 4b, the FET in air switches on at 15 V gate voltage, exhibiting an enhancement-mode behavior for the n-type semiconductor. Illuminated by UV light for 3 h and protected in Ar gas atmosphere, the surface adsorbed oxygen is desorbed. After the source-drain current is steady (UV light is turned off and still protected in Ar), the transfer characteristics of the FET is

DOI: 10.1021/acssensors.9b00259
ACS Sens. 2019, 4, 1577−1585

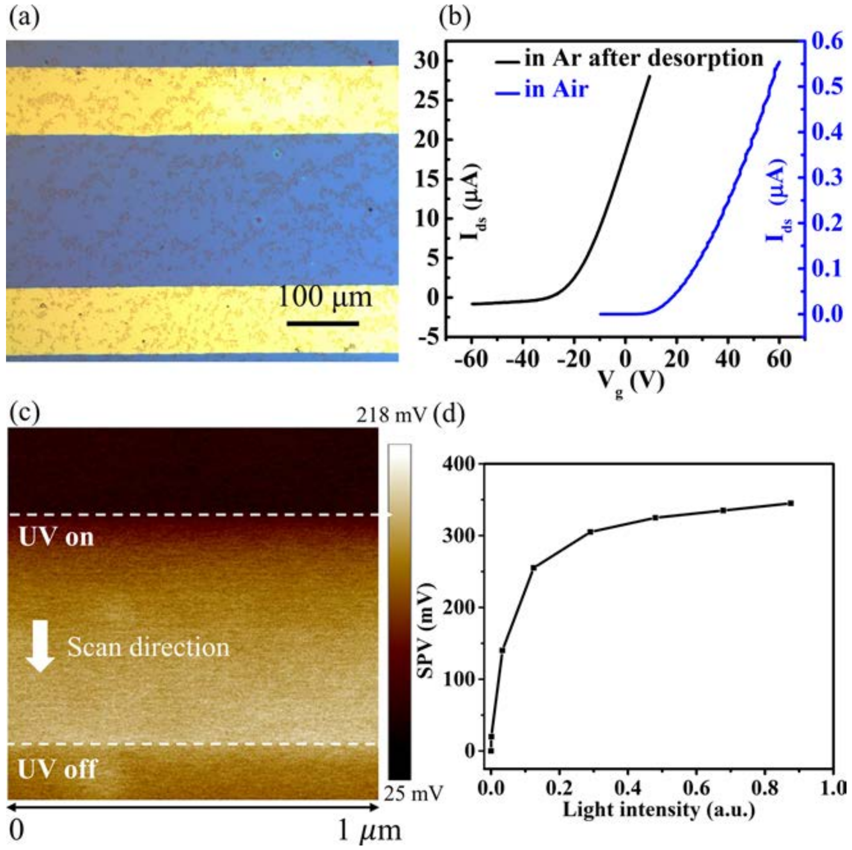

Figure 4. FET and KPFM characterization of ZnO nanofilm: (a) the optical image of ZnO nanofilm FET shows the distance between electrodes is 300 μm; (b) the threshold gate voltage shifts from 15 V to −25 V when the surface O_2 is desorbed and the FET is protected in Ar; (c) the surface potential of ZnO nanofilm is 45 mV in dark, and the UV light illumination leads to the increase of surface potential, which means the work function of ZnO is reduced; (d) the relationship between the SPV of ZnO nanofilm and the intensity of UV light.

measured. The FET is depleted at −25 V gate voltage, exhibiting the typical behavior of an n-type semiconductor. This positive shift of threshold voltage when oxygen molecules adsorbed can be attributed to the complete depletion of the ZnO nanofilm led by the adsorption of O_2, since totally depleted, the ZnO nanofilm is positively charged and requires a positive gate voltage to compensate for the positive charges inside.[22]

To quantify the distance between the Fermi level and conduction band of ZnO nanofilm, the surface potential of ZnO nanofilm in the dark and under UV light illumination is measured with KPFM, as shown in Figure 4c. In the dark, the surface potential (SP) of ZnO nanofilm is 45 mV. Calibrated with highly oriented pyrolytic graphite (HOPG), which has a known work function of 4.65 eV[27] and a measured SP of 60 mV, the SP of ZnO nanofilm corresponds to a work function of 4.665 eV. Taking the electron affinity of ZnO (4.30 eV) into consideration,[28] the distance between the Fermi level and surface conduction band ($E_C^s - E_f$) is 0.365 eV. Illumination of UV light leads to the increase of the ZnO nanofilm's SP, which corresponds to a decrease of work function, i.e., a decrease of the distance between Fermi level and conduction band. The change of SP caused by light illumination, defined as the surface photovoltage (SPV), is related to the light intensity. When UV light with enough intensity is applied, the surface adsorbed oxygen molecules are totally desorbed, which results in the almost disappearance of surface band bending and a decreased distance between the Fermi level and conduction band. The measured result is shown in Figure 4d. The SPV is 345 mV when te UV light intensity is enough and the work function of ZnO nanofilm under UV is 4.320 eV, which indicates the distance between the Fermi level and bulk conduction band ($E_C^b - E_f$) is 0.02 eV, taking the almost vanished surface band bending into consideration. The corresponding electron concentration of ZnO nanofilm under UV light illumination is $2.3 \times 10^{18}/\text{cm}^3$, calculated by $n = N_C \exp[-(E_C^b - E_f)/k_BT]$.

Numerical Simulation. The SPV of ZnO nanofilm is a combination of the change of surface band bending ($E_C^s - E_C^b$) and the change of the Fermi level's position ($E_C^b - E_f$). To quantify the surface band bending and the Fermi level's position from the measured SPV, the distributions of potential and carrier concentration need to be taken into consideration, which are governed by the space charge model:[29,30]

$$\Delta V(\vec{r}) = -\frac{\rho(\vec{r})}{\varepsilon\varepsilon_0} \tag{17}$$

$$\rho(\vec{r}) = q(n_D^+ - p_A^- + p(\vec{r}) - n(\vec{r})) \tag{18}$$

$$-en_s = \varepsilon_b\varepsilon_0\frac{dV}{dr}(r = 0) \tag{19}$$

where $V(\vec{r})$ is the potential, defined as $E_f - E_C^b - E_C^s$ (V is zero when the band is flat, and negative when the band bends upward), r is the distance from the core of ZnO nanoparticle, $\rho(\vec{r})$ is the charge density at r, n_D^+, p_A^-, $p(\vec{r})$, $n(\vec{r})$ are the concentration of donor, acceptor, hole, and electron,

DOI: 10.1021/acssensors.9b00259
ACS Sens. 2019, 4, 1577−1585

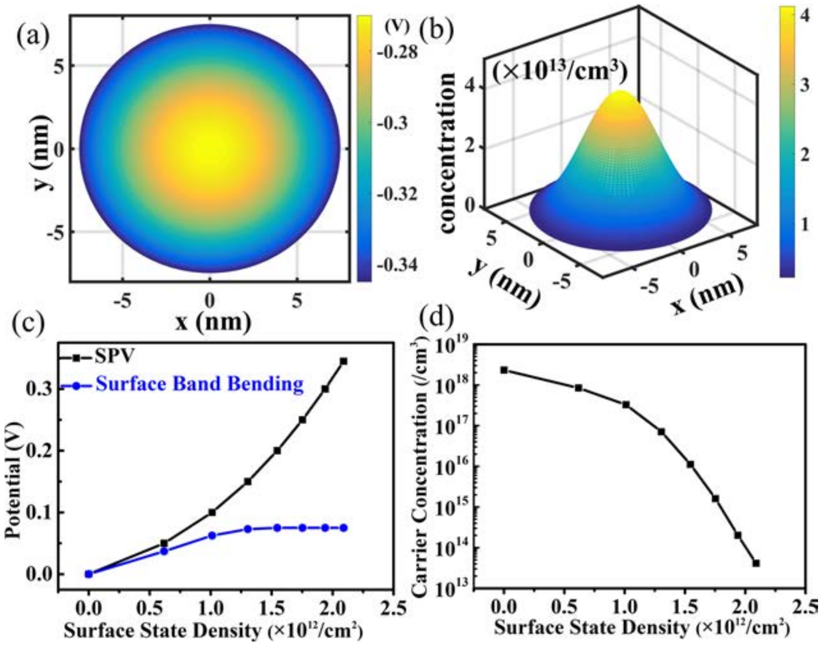

Figure 5. Distributions of (a) potential and (b) carrier concentration in ZnO nanoparticle in the dark. The depletion of whole nanoparticle is revealed by the negatively potential and the low carrier concentration ($4.1 \times 10^{13}/\text{cm}^3$) at the core of nanoparticle. (c) The SPV, surface band bending, and (d) the carrier concentration at core are all related to the surface state density. With the increase of surface state density, the SPV increases, the surface band bending stabilizes at 0.075 eV, and the carrier concentration dramatically reduces.

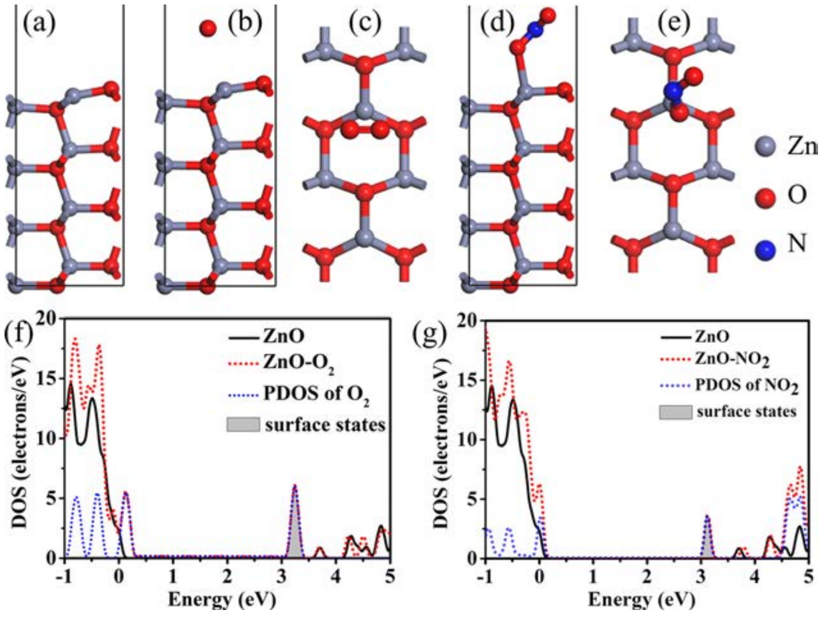

Figure 6. Optimized geometric configurations of (a) ZnO, (b, c) ZnO with O_2 adsorbed and (d, e) ZnO with NO_2 adsorbed. Panels a, b, d are from a sectional view which is perpendicular to the ZnO(100) surface, while panels c and e are from top view which only show the top atoms of ZnO. (f, g) Comparison of the DOS of the systems (free ZnO(100) surface, ZnO surface with adsorbates) and the PDOS of the adsorbates (O_2 and NO_2). The extrinsic surface states are indexed by the shadow area.

respectively. n_s is the surface state density, and ε_b and ε_0 are the dielectric constants of ZnO and vacuum. The concentration of impurity is assumed to be constant in the whole ZnO nanoparticle and can be obtained using the electric neutrality condition in the core of nanoparticle. The concentrations of electron and hole follow the Maxwell–Boltzmann approximation.

Since the depth of depletion layer is larger than the radius of nanoparticle 7.5 nm as measured by AFM, the whole nanoparticle has been depleted by surface adsorbed molecules. Because of the symmetry, the following boundary conditions are used: $V(0) = -\text{SPV}$, $V(d) = 0$, where d is the radius of nanoparticle. Using the 345 mV SPV measured by KPFM, the distributions of potential and carrier concentration across the ZnO nanoparticle in the dark and under UV light illumination are calculated. Figure 5a,b shows the distributions of potential and carrier concentration in the dark. Because of the depletion of the whole nanoparticle, the core has a negative potential (positively charged), the distance between Fermi level and conduction band $E_C^b - E_f$ increases from 0.02 to 0.27 eV, the surface band bending $E_C^s - E_C^b$ increase from 0.005 to 0.075 eV, and the carrier concentration reduced from $2.3 \times 10^{18}/\text{cm}^3$ to $4.1 \times 10^{13}/\text{cm}^3$, all compared with that of ZnO nanofilm under UV light illumination. The surface state density of adsorbed O_2 in dark is $2.1 \times 10^{12}/\text{cm}^2$.

The variation of surface state density would result in the change of SPV, which influences the surface band bending and carrier concentration as shown in Figure 5c,d. With the increase of surface state density, the surface band bending $E_C^s - E_C^b$ increases and stabilizes at 0.075 eV, while the distance between the Fermi level and conduction band $E_C^b - E_f$ keeps increasing, which corresponds to the depletion of whole ZnO nanoparticle, as illustrated by the decrease of carrier concentration by 5 orders of magnitude.

To calculate the binding energy and the position of surface state, first principle calculation is used. Geometric optimizations were performed employing density functional theory.[31−34] Generalized gradient approximation (GGA) in the scheme of Perdew−Burke−Ernzerhof (PBE) is used to describe the exchange-correlation.[35] 380 eV for the plane-wave cutoff, 8 × 5 × 1 Monkhorst−Pack sampling are used, and the system was fully relaxed until the final force was less than 0.01 eV/Å on each atom. The NO_2 and O_2 molecules were optimized in a 15 × 15 × 15 Å^3 sized cell. ZnO surfaces were modeled by period slabs using supercell with eight ZnO layers and vacuum space of 15 Å. The optimized geometric configurations of ZnO, ZnO with O_2 adsorbed, and ZnO with NO_2 adsorbed are shown in Figure 6a−e, where panels a, b, d are from a sectional view which is perpendicular with the ZnO(100) surface, while panels c and e are from top view which only show the top atoms of ZnO.

The ZnO(100) surface is known to exhibit a tilt of the Zn−O dimer,[36] as shown in Figure 6a. The adsorption of O_2 has no effect on this tilt, while the adsorption of NO_2 dramatically reduces the tilt of Zn−O dimer, which evidences the much larger binding energy of NO_2 than that of O_2 and is characterized by a bond between the N atom and the O atom of ZnO. The binding energy is calculated by the following formula:

$$\Delta E_{\text{ads}} = [(E_{\text{ZnO}} + E_{\text{ads}}) - E_{(\text{ads/ZnO})}] \tag{20}$$

where ΔE_{ads} is the binding energy, E_{ZnO} is the total energy of the clean ZnO surface, E_{ads} is the total energy of the NO_2 or O_2 molecule, $E_{(\text{ads/ZnO})}$ is the total energy of the ads/ZnO system (where ads is NO_2 or O_2). The calculated binding energy of O_2 is 0.18 eV and that of NO_2 is 0.46 eV.

To determine the position of extrinsic surface states caused by the adsorption, the density of states (DOS) of the systems (free ZnO (100) surface, ZnO surface with adsorbates) and the partial density of states (PDOS) of the adsorbates (O_2 and NO_2) are compared. The conduction bands are shifted by a "scissor operator" to adjust the band gap to the measured value.[37] As shown in Figure 6c,d, extrinsic surface states are introduced by the adsorbates, which locates around 0.35 eV below the valence band, indicated by the shadow area.

Finally, the factors that have influence on the adsorption in the modified Wolkeinstein's model have all been determined. The surface state density of the ZnO nanofilm sensor under different situations are calculated according to eqs 12−16. Since the position of the Fermi level is lower than that of the extrinsic surface state when the surface is saturated with adsorbed O_2, the further adsorption of NO_2 without UV illumination is dominated by the weak situation; thus, the surface state density of NO_2 without UV illumination is regarded as zero. The carrier concentration and surface band bending of the ZnO nanofilm sensor under different situations are calculated by the space charge model, with the respective surface state densities taken into consideration. Results are shown in Table 1. Gas sensitivity S_1 is the response of ZnO nanofilm to the NO_2 in the dark, UV sensitivity S_2 is the response to the UV light illumination in air, and gas sensitivity S_3 corresponds to the response to the NO_2 under UV light illumination. Since the resistance of ZnO nanofilm is determined by the carrier concentration and the surface band bending (which serves as a potential barrier between ZnO nanoparticles), the sensitivity is determined by the change of the carrier concentration and the change of surface band bending, which can be calculated by the following equations:

Table 1. Surface State Density, Carrier Concentration, Surface Band Bending, and Sensitivity in Different Situations

	in air in dark	in NO_2/air in dark	in air under UV	in NO_2/air under UV
surface state density (cm^{-2})	2.1×10^{12}	2.1×10^{12}	6.8×10^{10}	1.3×10^{12}
carrier concentration at core (cm^{-3})	4.1×10^{13}	4.1×10^{13}	2.3×10^{18}	5.0×10^{16}
surface band bending (eV)	0.075	0.075	0.005	0.075
simulated sensitivity		$S_1 = 1$	$S_2 = 0.8 \times 10^6$	$S_3 = 686$
experimental sensitivity		$S_1 = 10$	$S_2 = 1.4 \times 10^6$	$S_3 = 575$

$$S_1 = \frac{n_1}{n_2} \exp\left(\frac{\phi_2 - \phi_1}{k_B T}\right) \tag{21}$$

$$S_2 = \frac{n_3}{n_1} \exp\left(\frac{\phi_1 - \phi_3}{k_B T}\right) \tag{22}$$

$$S_3 = \frac{n_3}{n_4} \exp\left(\frac{\phi_4 - \phi_3}{k_B T}\right) \tag{23}$$

where n and ϕ refer to the carrier concentration and the surface band bending of ZnO nanofilm under different conditions: n_1 and ϕ_1 are that in air and the dark, n_2 and ϕ_2 are that in NO_2/air mixed gas and the dark, n_3 and ϕ_3 are that in air and under UV light illumination, and n_4, ϕ_4 are that in NO_2/air mixed gas and under UV light illumination. In the dark, the adsorption of O_2 leads to the depletion of whole ZnO nanofilm, as characterized by the low carrier concentration. Further adsorption of NO_2 on ZnO nanofilm has no effect on the surface state density, carrier concentration, and the surface band bending. Thus, the gas sensitivity of ZnO nanofilm is quite low. The illumination of UV light leads to the desorption of adsorbed O_2 (surface state density decreases from $2.1 \times 10^{12}/\text{cm}^2$ to $6.8 \times 10^{10}/\text{cm}^2$), a dramatic increase of carrier concentration, and the disappearance of the surface band bending, as evidenced by the UV sensitivity with 6 orders of magnitude. As to the situation with both NO_2 and UV illumination, adsorption of NO_2 leads to the increase of surface

DOI: 10.1021/acssensors.9b00259
ACS Sens. 2019, 4, 1577−1585

state density (from $6.8 \times 10^{10}/\text{cm}^2$ to $1.3 \times 10^{12}/\text{cm}^2$), which reduces the carrier concentration and rebuilds the surface band bending. The simulated sensitivities in different situations agree well with the experimental values, which proves that the gas sensitivity enhancement of the ZnO nanofilm gas sensor should be ascribed to the more dramatic increase of surface state density and surface band bending activated by UV light illumination compared with that in the dark.

Although NO_2 gas has a greater binding energy than O_2 on the ZnO surface, the adsorption of O_2 molecules in the dark combined with the limited size of the nanoparticle leads to the full depletion in ZnO and a higher energy level of surface state compared with the Fermi level. These factors dramatically restrict the further adsorption of NO_2 molecules in the dark. In other words, electrons in ZnO are not available for the "strong" adsorption of NO_2 molecules, which means the NO_2 gas in the dark basically has no influence on the resistance of ZnO nanoparticle and the surface barrier height. As a result, the sensitivity of ZnO nanofilm to NO_2 gas in dark is quite low. When illuminated by UV light, a new equilibrium between gas molecules and carriers in ZnO is formed by three steps. First, the combination of photogenerated holes and adsorbed O_2 molecules leads to the release of electrons in ZnO, the flattening of surface band bending, and the return of the surface state to the position below the Fermi level. To form a "strong" adsorption, NO_2 and O_2 molecules are now freely competing for electrons in ZnO which is determined by their respective binding energy. The larger binding energy of NO_2 gas grants it a larger surface state density which gradually depletes the electrons in ZnO and raises the position of surface states until a new equilibrium is formed. Similar with the situation in the dark, the ZnO is depleted and a surface barrier is formed between ZnO nanoparticles, but they are mainly attributed to the large surface state density of adsorbed NO_2 molecules rather than that of O_2. As a result, the sensitivity of ZnO nanofilm gas sensor to NO_2 is activated and enhanced by the UV light illumination.

■ CONCLUSION

In summary, the influence of UV light illumination on the surface state densities of adsorbed O_2 and NO_2 molecules are quantified according to a modified Wolkenstein's model and the space charge model. The adsorption process in different situations is mainly determined by the following factors: the surface band bending and Fermi level of ZnO nanofilm, the binding energy and extrinsic surface state of adsorbates, and the depletion of whole semiconductor caused by the finite size. With all these factors taken into consideration, good agreement is reached between the simulated sensitivity and the experimental results both in the dark and under UV light illumination. The enhancement of ZnO nanofilm gas sensor by UV light illumination is ascribed to the change of surface state density and surface band bending. In the dark, no obvious change is induced when NO_2 is introduced into the atmosphere, which leads to a low sensitivity. While under UV light illumination, the adsorption of NO_2 leads to the surface state density changes from 6.8×10^{10} cm^{-2} to 1.3×10^{12} cm^{-2}, and the surface band bending changes from 0.005 to 0.075 eV. The combination of these factors results in the enhancement of sensitivity led by UV light illumination.

■ AUTHOR INFORMATION

Corresponding Author

*E-mail: qinyong @lzu.edu.cn.

ORCID

Yong Qin: 0000-0002-6713-480X

Author Contributions

[#]G.L. and Z.S. are cofirst authors who contributed equally to this work. Y.Q. conceived and designed the experiments. G.L. conceived the model and performed the simulation. Z.S. performed the experiments. D.Z. fabricated the devices. Q.X. fabricated the materials. L.M. tested the gas sensors.

Notes

The authors declare no competing financial interest.

■ ACKNOWLEDGMENTS

We sincerely appreciate the support from NSFC (No. 51472111), the National Program for Support of Top-notch Young Professionals, and the Fundamental Research Funds for the Central Universities (No. lzujbky-2018-ot04).

■ REFERENCES

(1) Ra, H. W.; Choi, K. S.; Kim, J. H.; Hahn, Y. B.; Im, Y. H. Fabrication of ZnO nanowires using nanoscale spacer lithography for gas sensors. *Small* **2008**, *4* (8), 1105−1109.

(2) Na, C. W.; Woo, H. S.; Kim, I. D.; Lee, J. H. Selective detection of NO_2 and C_2H_5OH using a Co_3O_4-decorated ZnO nanowire network sensor. *Chem. Commun.* **2011**, *47* (18), 5148−5150.

(3) Qiu, Y.; Yang, S. ZnO Nanotetrapods: Controlled Vapor-Phase Synthesis and Application for Humidity Sensing. *Adv. Funct. Mater.* **2007**, *17* (8), 1345−1352.

(4) Lu, G.; Xu, J.; Sun, J.; Yu, Y.; Zhang, Y.; Liu, F. UV-enhanced room temperature NO_2 sensor using ZnO nanorods modified with SnO_2 nanoparticles. *Sens. Actuators, B* **2012**, *162* (1), 82−88.

(5) Fan, S.-W.; Srivastava, A. K.; Dravid, V. P. UV-activated room-temperature gas sensing mechanism of polycrystalline ZnO. *Appl. Phys. Lett.* **2009**, *95* (14), 142106.

(6) de Lacy Costello, B. P. J.; Ewen, R. J.; Ratcliffe, N. M.; Richards, M. Highly sensitive room temperature sensors based on the UV-LED activation of zinc oxide nanoparticles. *Sens. Actuators, B* **2008**, *134* (2), 945−952.

(7) Liang, X.; Dong, R.; Ho, J. C. Self-Assembly of Colloidal Spheres toward Fabrication of Hierarchical and Periodic Nanostructures for Technological Applications. *Advanced Materials Technologies* **2019**, *4* (3), 1800541.

(8) Das, S.; Hossain, M. J.; Leung, S.-F.; Lenox, A.; Jung, Y.; Davis, K.; He, J.-H.; Roy, T. A leaf-inspired photon management scheme using optically tuned bilayer nanoparticles for ultra-thin and highly efficient photovoltaic devices. *Nano Energy* **2019**, *58*, 47−56.

(9) Su, Y.; Xie, G.; Tai, H.; Li, S.; Yang, B.; Wang, S.; Zhang, Q.; Du, H.; Zhang, H.; Du, X.; Jiang, Y. Self-Powered Room Temperature NO 2 Detection Driven by Triboelectric Nanogenerator under UV illumination. *Nano Energy* **2018**, *47*, 316−324.

(10) Xu, J.; Han, J.; Zhang, Y.; Sun, Y. a.; Xie, B. Studies on alcohol sensing mechanism of ZnO based gas sensors. *Sens. Actuators, B* **2008**, *132* (1), 334−339.

(11) Fan, S.-W.; Srivastava, A. K.; Dravid, V. P. Nanopatterned polycrystalline ZnO for room temperature gas sensing. *Sens. Actuators, B* **2010**, *144* (1), 159−163.

(12) Park, S.; An, S.; Mun, Y.; Lee, C. UV-enhanced NO2 gas sensing properties of SnO2-core/ZnO-shell nanowires at room temperature. *ACS Appl. Mater. Interfaces* **2013**, *5* (10), 4285−4292.

(13) Zhai, J.; Wang, T.; Wang, C.; Liu, D. UV-light-assisted ethanol sensing characteristics of g-C 3 N 4 /ZnO composites at room temperature. *Appl. Surf. Sci.* **2018**, *441*, 317−323.

(14) Medina, H.; Li, J.-G.; Su, T.-Y.; Lan, Y.-W.; Lee, S.-H.; Chen, C.-W.; Chen, Y.-Z.; Manikandan, A.; Tsai, S.-H.; Navabi, A.; Zhu, X.;

Shih, Y.-C.; Lin, W.-S.; Yang, J.-H.; Thomas, S. R.; Wu, B.-W.; Shen, C.-H.; Shieh, J.-M.; Lin, H.-N.; Javey, A.; Wang, K. L.; Chueh, Y.-L. Wafer-Scale Growth of WSe2Monolayers Toward Phase-Engineered Hybrid WOx/WSe2 Films with Sub-ppb NOx Gas Sensing by a Low-Temperature Plasma-Assisted Selenization Process. *Chem. Mater.* **2017**, *29* (4), 1587−1598.

(15) Wang, H.; Periyanagounder, D.; Li, A.; He, J. Fabrication of Silicon Hierarchical Structures for Solar Cell Applications. *IEEE Access* **2019**, *7*, 19395−19400.

(16) Ma, Y.; Gao, W.; Zhang, Z.; Zhang, S.; Tian, Z.; Liu, Y.; Ho, J. C.; Qu, Y. Regulating the surface of nanoceria and its applications in heterogeneous catalysis. *Surf. Sci. Rep.* **2018**, *73* (1), 1−36.

(17) Alenezi, M. R.; Alshammari, A. S.; Jayawardena, K. D.; Beliatis, M. J.; Henley, S. J.; Silva, S. R. Role of the Exposed Polar Facets in the Performance of Thermally and UV Activated ZnO Nanostructured Gas Sensors. *J. Phys. Chem. C* **2013**, *117* (34), 17850−17858.

(18) Peng, L.; Xie, T.-F.; Yang, M.; Wang, P.; Xu, D.; Pang, S.; Wang, D.-J. Light induced enhancing gas sensitivity of copper-doped zinc oxide at room temperature. *Sens. Actuators, B* **2008**, *131* (2), 660−664.

(19) Saboor, F. H.; Ueda, T.; Kamada, K.; Hyodo, T.; Mortazavi, Y.; Khodadadi, A. A.; Shimizu, Y. Enhanced NO_2 gas sensing performance of bare and Pd-loaded SnO_2 thick film sensors under UV-light irradiation at room temperature. *Sens. Actuators, B* **2016**, *223*, 429−439.

(20) Zhang, C.; Geng, X.; Liao, H.; Li, C.-J.; Debliquy, M. Room-temperature nitrogen-dioxide sensors based on ZnO 1−x coatings deposited by solution precursor plasma spray. *Sens. Actuators, B* **2017**, *242*, 102−111.

(21) Wolkenstein, T. *Electronic Processes on Semiconductor Surfaces during Chemisorption*; Consultants Bureau: New York, 1991; p 444.

(22) Li, G.; Meng, L.; Zhu, X.; Gao, W.; Qin, Y.; Chen, L. Clarifying the high on/off ratio mechanism of nanowire UV photodetector by characterizing surface barrier height. *Nanoscale* **2018**, *10* (5), 2242−2248.

(23) Rothschild, A.; Komem, Y. Numerical computation of chemisorption isotherms for device modeling of semiconductor gas sensors. *Sens. Actuators, B* **2003**, *93* (1−3), 362−369.

(24) Gümüş, C.; Ozkendir, O. M.; Kavak, H.; Ufuktepe, Y. Structural and optical properties of zinc oxide thin films prepared by spray pyrolysis method. *J. Optoelectronics Adv. Mater.* **2006**, *8*, 299−303.

(25) Koida, T.; Chichibu, S. F.; Uedono, A.; Tsukazaki, A.; Kawasaki, M.; Sota, T.; Segawa, Y.; Koinuma, H. Correlation between the photoluminescence lifetime and defect density in bulk and epitaxial ZnO. *Appl. Phys. Lett.* **2003**, *82* (4), 532−534.

(26) Meyers, S. T.; Anderson, J. T.; Hung, C. M.; Thompson, J.; Wager, J. F.; Keszler, D. A. Aqueous Inorganic Inks for Low-Temperature Fabrication of ZnO TFTs. *J. Am. Chem. Soc.* **2008**, *130* (51), 17603−17609.

(27) Palma, M.; Levin, J.; Lemaur, V.; Liscio, A.; Palermo, V.; Cornil, J.; Geerts, Y.; Lehmann, M.; Samorì, P. Self-Organization and Nanoscale Electronic Properties of Azatriphenylene-Based Architectures: A Scanning Probe Microscopy Study. *Adv. Mater.* **2006**, *18* (24), 3313−3317.

(28) Sohn, J. I.; Cha, S. N.; Song, B. G.; Lee, S.; Kim, S. M.; Ku, J.; Kim, H. J.; Park, Y. J.; Choi, B. L.; Wang, Z. L.; Kim, J. M.; Kim, K. Engineering of efficiency limiting free carriers and an interfacial energy barrier for an enhancing piezoelectric generation. *Energy Environ. Sci.* **2013**, *6* (1), 97−104.

(29) Kronik, L.; Shapira, Y. Surface photovoltage phenomena: theory, experiment, and applications. *Surf. Sci. Rep.* **1999**, *37* (1−5), 1−206.

(30) Soudi, A.; Hsu, C. H.; Gu, Y. Diameter-dependent surface photovoltage and surface state density in single semiconductor nanowires. *Nano Lett.* **2012**, *12* (10), 5111−5116.

(31) Hohenberg, P.; Kohn, W. Inhomogeneous electron gas. *Phys. Rev.* **1964**, *136*, B864−B871.

(32) Kohn, W.; Sham, L. J. Self-consistent equations including exchange and correlation effects. *Phys. Rev.* **1965**, *140*, A1133−A1138.

(33) Payne, M. C.; Teter, M. P.; Allan, D. C.; Arias, T. A.; Joannopoulos, J. D. Iterative minimization techniques for ab initio total-energy calculations - molecular-dynamics and conjugate gradients. *Rev. Mod. Phys.* **1992**, *64*, 1045−1097.

(34) Clark, S. J.; Segall, M. D.; Pickard, C. J.; Hasnip, P. J.; Probert, M. J.; Refson, K.; Payne, M. C. First principles methods using CASTEP. *Z. Kristallogr. - Cryst. Mater.* **2005**, *220*, 567−570.

(35) Perdew, J. P.; Ruzsinszky, A.; Csonka, G. I.; Vydrov, O. A.; Scuseria, G. E.; Constantin, L. A.; Zhou, X.; Burke, K. Restoring the density-gradient expansion for exchange in solids and surfaces. *Phys. Rev. Lett.* **2008**, *100* (13), 136406.

(36) Meyer, B.; Marx, D. Density-functional study of the structure and stability of ZnO surfaces. *Phys. Rev. B: Condens. Matter Mater. Phys.* **2003**, *67* (3), No. 035403.

(37) Laskowski, R.; Christensen, N. E. Ab initiocalculation of excitons in ZnO. *Phys. Rev. B: Condens. Matter Mater. Phys.* **2006**, *73* (4), No. 045201.